CHAPTER

1

IS ONE ENOUGH?

ANDREW C. BEVERIDGE, JAMES H. JETT, AND RICHARD A. KELLER

1.1. INTRODUCTION

A concern often expressed about single-molecule measurements can be stated as, "Single-molecule measurements are 'cool' but what good are they if you have to measure a million single molecules to estimate the properties of the system?" This is a reasonable concern. Thus, a major focus of this chapter is modeling the effect of sample size (typically a few molecules) on the accuracy of analytical measurements and the extrapolation of properties measured at the single-molecule level to properties derived from ensemble measurements. We include a summary of DNA fingerprinting of single viral particles and bacterial cells that demonstrates that only a few measurements are required. The contrast between single-molecule and bulk measurements is that single-molecule measurements yield physical properties of *individual* molecules whereas individual molecular properties are difficult or impossible to obtain from bulk measurements; often the heterogeneous nature of single measurements is masked in bulk systems. We finish with (a) a description of "virtual sorting," where the data stream is sorted instead of the sample stream, and (b) the implementation of virtual sorting to statistical chemistry to either eliminate or reduce the necessity to purify a sample.

1.1.1. Significance of a Single-Molecule Measurement

There is a fundamental postulate of statistical mechanics that states, "The (long) time average of a mechanical property M in the thermodynamic system of interest is equal to the ensemble average of M, in the limit as N goes to infinity" (Hill, 1960). (Here and throughout this chapter, N refers to the number of molecules.) If this true, and indeed it must be, why do single-molecule experiments? It is clear that the average fluorescence intensity of a single molecule recorded over many cycles, as it undergoes changes between a fluorescent species and a nonfluorescent species, is equivalent to the average intensity from multiple molecules over one cycle.

We address two different but related aspects of this postulate: (1) How many times should the same single molecule be analyzed for the measured value(s) to be a good representation of the ensemble average? (2) Can single-molecule properties be extracted from bulk data?

The first question relates to studying the properties of single molecules free from averaging effects associated with bulk measurements. A good example is the quantification of the

New Frontiers in Ultrasensitive Bioanalysis. Edited by Xiao-Hong Nancy Xu

thermodynamics and dynamics of protein folding where subtle differences in the response curves indicate the presence of multiple folding pathways, barriers in the exit channel, and deviations from a simple two-state model, which are hidden in ensemble measuements (Schenter et al., 1999; Yang and Xie, 2002a,b; Yang and Cao, 2001). A related question is, How many identical single molecules are needed to estimate a sample's composition? For example, DNA fingerprinting for pathogen detection and identification by gel electrophoresis typically takes several days. Most of the time is spent culturing the sample to acquire sufficient material for analysis. The ability to size accurately *single* DNA fragments reduces sample preparation time considerably (Ferris et al., 2005; Larson et al., 2000). A similar problem exists with nonculturable bacteria where it is difficult to grow enough sample for standard analyses (Leadbetter, 2003; Pennisi, 2004).

The second question—How can you extract single-molecule properties from data collected from probe volumes that contain more than one emitting molecule?—is more difficult. The magnitude of the problem is apparent by looking at Figure 1.1, which shows time-dependent fluorescence intensity fluctuations as a function of the number of molecules in the probe volume. Even for two molecules, it is impossible to deconvolute the signal into the contribution from each molecule.

It is often stated that the difference between single-molecule and ensemble measurements is just a synchronization problem; but it is more than a synchronization problem. Due to the stochastic nature of fundamental processes, following a synchronized start, the molecules

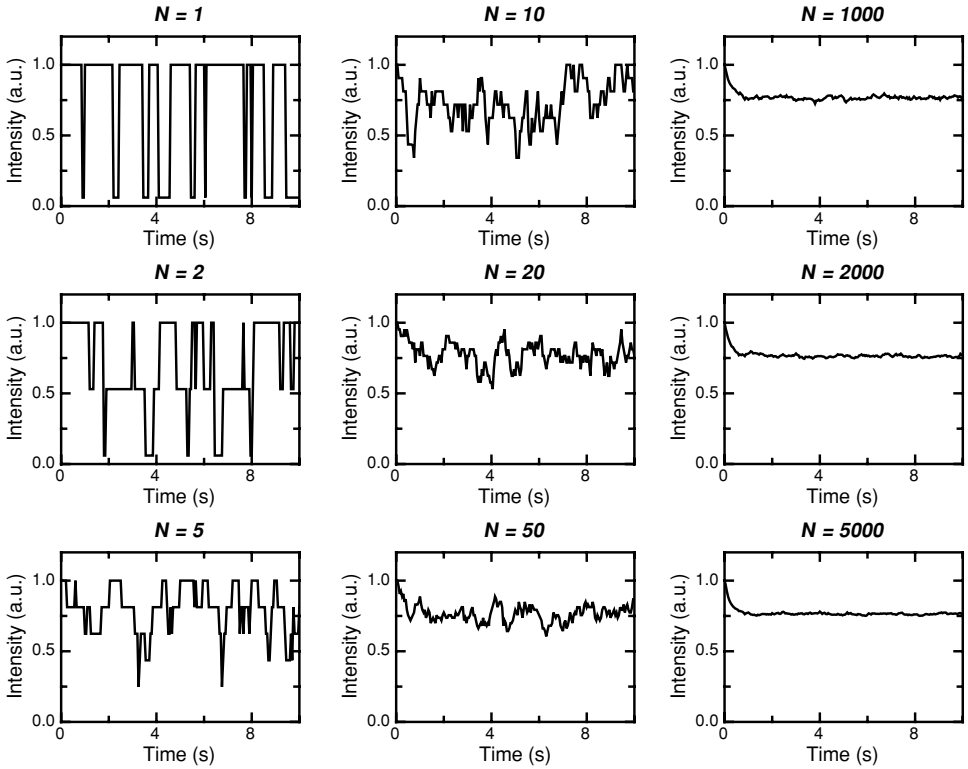

Figure 1.1. Simulated data stream for the fluorescence intensity from N molecules in the probe volume. The parameters for the simulation are listed in Table 1.1. Note that the intensity in each plot is normalized and that all the molecules start in the "on" state. The number of molecules present in the probe volume varies from 1 to 5000.

Table 1.1. Values for the Simulations Computed Here

Species	$k(s^{-1})$	τ (s)	Intensity
A	1.111	0.9	1.00
B	3.333	0.3	0.06

k is the rate constant, τ is the inverse of k (that is, the lifetime of the state), and the intensity represents the fluorescence intensity of each state. The average cycle time, τ_{cyc}, is 1.2 s and the mean fluorescence intensity is 0.765.

get "out of step" in approximately one cycle and distributions of the measured parameters of the sample are difficult to discern. Fortunately, properties of the system can be measured without a synchronous start.

1.2. MODEL SYSTEM

1.2.1. Equilibrium and Kinetics

We choose a simple system of a nondiffusing single molecule oscillating between a strongly fluorescent state and a weakly fluorescent state to characterize the particularities associated with the study of single molecules in small probe volumes. We focus on the problems and opportunities that result from using probe volumes less than or equal to a femtoliter. Equations (1.1a) and (1.1b) describe the equilibrium behavior of two conformations of the same molecule, A and B:

$$\mathrm{A} \underset{k_2}{\overset{k_1}{\rightleftharpoons}} \mathrm{B} \tag{1.1a}$$

$$K_{\mathrm{eq}} = \frac{[\mathrm{B}]}{[\mathrm{A}]} = \frac{k_1}{k_2}, \tag{1.1b}$$

where [A] and [B] are the respective concentrations of each species, k_1 and k_2 are the rate constants, and K_{eq} is the equilibrium constant. For a small displacement from equilibrium, the differential rate law is

$$\frac{d\Delta f_A(t)}{dt} = -(k_1 + k_2)\Delta f_A(t) = -\frac{d\Delta f_B(t)}{dt}, \tag{1.2}$$

where $\Delta f_A(t)$ and $\Delta f_B(t)$ denote the deviation of the concentration from equilibrium for species A and B at time t. For the closed, two-state system modeled here, the sum of [A] plus [B] is constant; thus $\Delta f_A(t)$ equals $-\Delta f_B(t)$. The solution to Eq. (1.2) is

$$\Delta f_A(t) = \Delta f_A^0 \exp[-(k_1 + k_2)t], \tag{1.3}$$

where Δf_A^0 is the initial deviation from equilibrium (Cantor and Schimmel, 1980). The probability of finding the system in A or B is

$$P_A = \frac{k_2}{k_1 + k_2}, \qquad P_B = \frac{k_1}{k_1 + k_2}, \tag{1.4}$$

where P_A and P_B are the probabilities for A and B, respectively. The mean fluorescence intensity, $\langle I_f \rangle$, is given by

$$\langle I_f \rangle = \alpha\phi_A[\mathrm{A}] + \beta\phi_B[\mathrm{B}] = \alpha\phi_A N\frac{k_2}{k_1+k_2} + \beta\phi_B N\frac{k_1}{k_1+k_2}, \tag{1.5}$$

where α and β depend upon the absorption, emission, and detection factors for A and B, and ϕ_A and ϕ_B are the fluorescence quantum yields for A and B.

Single-molecule measurements of the system give k_1, k_2, I_A, and I_B; therefore the parameters α and β can usually be determined by calibration of the apparatus allowing one to obtain values for ϕ_A and ϕ_B.

1.2.2. Generation of Synthetic Data

The parameters used in the following Poisson simulation of a data stream (Demas, 1983; Matthews and Walker, 1964), chosen to represent a typical photophysical process, are listed in Table 1.1. The conclusions drawn from data synthesized from these particular values may change significantly for a different choice of parameters. Here a cycle is defined as the total of the time period that a molecule spends in each state.

$$\tau_{\mathrm{cyc}} = \tau_1 + \tau_2, \tag{1.6}$$

where τ_1 and τ_2 are the inverse of k_1 and k_2, and τ_{cyc} is the cycle time. The probability for the forward reaction in Eq. (1.1), $P(t)$, that A changes its conformation at time t within dt is

$$P(t) \approx k_1\,\mathrm{d}t. \tag{1.7}$$

The approximation is valid for small dt. For the simulation, a molecule changes states if a uniform random number is less than k_1dt. The reaction time is determined by the number of trials needed for a newly generated random number to meet the specified condition above; the number of trials is then multiplied by dt. In the case for simulations of multiple molecules, data from individual molecules were added together. In Figure 1.1, we choose to start all of the molecules in A in order to simulate a perturbation-jump experiment. Alternatively, when a random start is desired, a uniform random number is compared to one of the probabilities in Eq. (1.4) to determine in which state each molecule starts.

1.2.3. Data Analysis

1.2.3.1. Single Molecule in the Probe Volume

Figure 1.1, $N = 1$, is a simulation of the time-dependent fluorescence intensity for a single molecule, fixed in the probe volume, that oscillates between a fluorescent and a weakly fluorescent conformation; thermodynamic driving forces cause the molecule to change conformations. The time that the molecule spends in each conformation is stochastic. Confining the molecule to the probe volume is useful because it extends the range of kinetic

parameters that can be studied and improves the accuracy of the parameters extracted from fits of the data to curves derived from the reaction mechanism and eliminates complications due to diffusion (Baldini et al., 2005; Jia et al., 1999; Rhoades et al., 2003; Talaga et al., 2000). In practice, the sampling time is limited to less than 100,000 photon absorptions by photobleaching (Soper et al., 1993) and other considerations (Vazquez et al., 1998; Zander et al., 2002).

We describe three methods for data analysis when only one molecule is in the probe volume: (1) averaging, (2) autocorrelation, and (3) distribution analyses.

1. The time averages of the "on and off" periods are measured for a chosen number of cycles; the averages are then inverted to give the rate constants, k_1 and k_2. The rate constants then can be summed to give the relaxation time, $(k_1 + k_2)^{-1}$, of the system. Here, the assumption is made that differences between states are discernible such that their respective time dependence can be accurately determined (Verberk and Orrit, 2003).
2. The fluorescence autocorrelation function for a simple first-order kinetic process, undergoing fluctuations around the equilibrium concentration, exhibits an exponential decay with a decay rate that is the sum of the rate constants $(k_1 + k_2)$. This type of analysis is called fluorescence correlation spectroscopy (FCS). Autocorrelation requires an analysis time long enough for both states to be sampled such that their average is independent of the time—that is, constant within statistical variation. Note that the time to reach a stationary system is independent of the number of molecules in the system. The fluorescence intensity autocorrelation function is defined as

$$C(t) = \frac{\langle \delta I(t) \delta I(t+\tau) \rangle}{\langle I \rangle^2}, \tag{1.8}$$

   where δI are the zero-mean intensity fluctuations, $\delta I(t) = I(t) - \langle I \rangle$, at time t and $t + \tau$, respectively (Aragon and Pecora, 1976, Elson, 1985, Krichevsky and Bonnet, 2002, Zander et al., 2002).
3. Distribution analyses include both binning and cumulative distribution functions. In the binning method, "on and off" time periods are binned separately and plotted individually in histogram format; rate constants are determined from each histogram. For the simulations here, a minimum of 10 cycles is needed to define a rudimentary histogram. Alternatively, the data can be fit to the cumulative distribution function for the probability density function that describes the data. The cumulative distribution method has an advantage over binning in that as few as two to three points are needed. However, for cases more complicated than considered here, the cumulative distribution function may be difficult to compute analytically.

1.2.3.2. Multiple Molecules in the Probe Volume

In the study of biological systems within a fixed probe volume (cells, lipid vesicles, cell membranes, etc.), it is often of interest to determine the number of a particular species in the probe volume. The ability to measure the number of molecules and determine individual

molecular properties leads to new insights regarding basic intracellular functions. Here, two limits of multiple molecules in the probe volume are examined: a bulk system, $N > 10$, where discrete contributions from individual molecules are not apparent, and a system where discrete contributions from individual molecules are obvious, $2 \leq N \leq 10$, herein referred to as a "prebulk" system.

Figure 1.1 illustrates the change from single-molecule system to prebulk system to bulk system as N is increased from 1 to 5000. This corresponds to a concentration range from 1 nM to 10 μM for a probe volume of 1 fL. Although each molecule is in either A or B, the system is not constrained to a number normalized intensity of either 1 or 0.06 because the molecules get out of phase. For example, in the case where the number of molecules is five, all of the molecules must be in B for a normalized intensity of 0.06; this is improbable, approximately one out of a thousand, for the simulation parameters used here. For five molecules, six normalized intensities are possible with frequencies determined by probability theory. The corresponding plateaus are clearly visible for N equals 2 and 5, and occasionally 10 in Figure 1.1. Discrete steps are not evident for N greater than 10.

Bulk Systems and Synchronous Starts. Consider the simulations in Figure 1.1 for the bulk case. Here, at $t = 0$ all of the molecules are in A and relax to the equilibrium distribution in less than the average of one cycle. As stated previously, the simulations are analogous to rapid perturbation experiments—for example, optical pumping, temperature jump, pH jump, or the addition of an appropriate chemical. For this type of experiment, the time dependence of the signal relaxation gives the sum of the rate constants, $k_1 + k_2$, whereas the long-time limit of the signal gives the average fluorescence intensity as given in Eq. (1.5). In the special case where one of the states is "dark," the equilibrium constant is determined from the ratio of the intensity at time zero to the intensity at times greater than the chemical relaxation time. Depending on the type of experiment, bulk measurements give the equilibrium fluorescence intensity and the sum of the rate constants; individual values of I_A, I_B, k_1, and k_2 are typically difficult to measure.

Prebulk System. For the prebulk system we refer to two distinct states of the system: *all on* and *all off*. (There are a total of $N + 1$ distinct states; the number of configurations is $(A + B)^N$.) Here *all on* refers to the case where *every* molecule in the probe volume is A concurrently; correspondingly, *all off* indicates that every molecule is B at the same time. Assuming that all the fluorescing molecules in the probe volume are identical, probability theory predicts that the individual rate constants can be determined by the average of the period when *all the molecules* are either *all on* or *all off*; the average period multiplied by the number of molecules gives the inverse of the corresponding rate constant (Riley et al., 1997). This measurement depends on explicit knowledge of the number of molecules in the probe volume. Figure 1.2 gives an example for 2 to 10 molecules. Conversely, if the rate constants are known and assuming identical molecules, the average of either the *all on* or *all off* periods can be used to determine the number of molecules in the probe volume. If neither the rate constant nor the number of molecules is known, the ratio of the average lifetime of the *all off* state to the *all on* state gives the equilibrium constant. For all types of measurements in a prebulk system the system state must be known—that is, whether the system is in the *all on* or *all off* state. There are two possible experimental procedures that

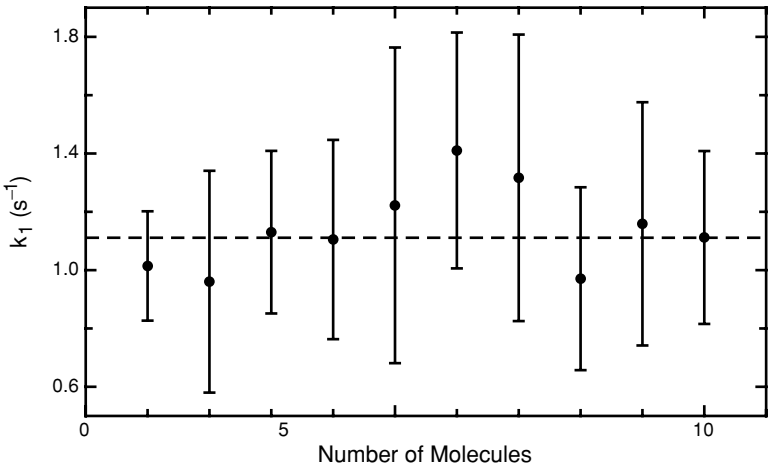

Figure 1.2. Determination of k_1 in a prebulk system from 1 to 10 identical molecules in the probe volume. The average of *all on* period is computed for a data stream where the average number of *all on* periods is 10 in the data stream; see Eq. (1.9). The average *all on* period is then multiplied by the number of molecules and inverted to give k_1. The error bars represent the standard deviation from 10 independent numeric simulations. The dashed line indicates the true value for k_1.

can be used with this method, and both methods can determine the system state:

1. If there is a distribution of N in the sample, then one can look for a probe volume where $N = 1$; then use the data to determine the rate constants. Once the rate constants are known, N can be determined for other probe volumes when N is less than or equal to 10.
2. After sufficient data are collected, the light intensity can be increased to facilitate photobleaching. For noninteracting molecules, photobleaching occurs in discrete steps; the steps are counted to determine N (Park et al., 2005). The rate constants can be calculated once N is known.

Table 1.2 gives the probabilities of finding the system in either *all on* or *all off* states as a function N for the parameters in Table 1.1. The time trajectory for either a simulation or an

Table 1.2. The Probabilities of Finding the System with Either *All the Molecules On* or *Off* as Function of the Number of Molecules for the Simulation Parameters of k_1 and k_2 Equal to 1.111 and 3.333s^{-1}, Respectively (see Table 1.1)[a]

Molecules	Probability (All On)	Probability (All Off)	Simulation Time (s) (All On)	Simulation Time (s) (All Off)
2	0.56	6.3×10^{-2}	8.0	14.0
4	0.32	3.9×10^{-3}	7.2	192.0
6	0.18	2.4×10^{-4}	8.5	2.1×10^{3}
8	0.10	1.5×10^{-5}	11.3	2.5×10^{4}
10	0.06	9.5×10^{-7}	16.0	3.2×10^{5}

[a]The simulation time is the time needed for either a simulation or real experiment, assuming one makes 10 measurements of either the "*all on* or *all off*" periods. Figure 1.2 is the determination of k_1 using the simulation times in this table.

experiment can be computed from the following formulae:

$$T_A = \left(\frac{m}{Nk_1}\right)(P_A)^{-N}, \tag{1.9a}$$

$$T_B = \left(\frac{m}{Nk_2}\right)(P_B)^{-N}, \tag{1.9b}$$

where T_A and T_B are the times needed to measure a specific number, m, of *all on* and *all off* periods. For example, we anticipate 10 separate periods of *all on* (*all off*) for $m = 10$. For the *all on* case where $N = 3$ and $m = 10$, along with the parameters in Table 1.1, T_A is 7.2 s; 100 independent simulations with the time set to 7.2 s give $m = 10.1 \pm 1.9$, which agrees with the initial premise of 10 independent measurements in the data stream. The interesting part of this method is that times are measured rather than intensities. Finally, autocorrelation analysis can also be applied to this system to determine the sum of the rate constants. Neither method requires a synchronous start.

1.2.4. Comparison of Data Analysis Techniques

Both averaging and distribution methods give the mean value of the histogram and the variance; thus there is little difference between the two. Because averaging analysis and distribution analysis are closely related, only the differences between the averaging method and autocorrelation analysis are considered; the differences between distribution and autocorrelation analyses are assumed to the be same as the former case.

The major difference between distribution analysis and averaging is that distribution analysis gives a visual representation of the values that may help distinguish between two distinct states, whereas averaging gives a single point. For example, the distinction between two closely separated peaks in a distribution analysis is evident, whereas the average would only give one point, the mean of the two peaks. In the limit of a normal distribution, averaging and distribution analysis give identical answers.

1.2.4.1. Single-Molecule Case

There is a fundamental difference between an autocorrelation analysis and measuring the distributions of on and off periods for the case where both states are fluorescent. The time dependence of the autocorrelation of the fluorescence intensity fluctuations provides the sum of the forward and reverse reaction rate constants; in the special case, where only one state is fluorescent and the other state is dark, the zero-time offset gives the equilibrium constant (Zander et al., 2002). However, the averaging method gives rate constants for each state even if both states are fluorescent. In addition, the averaging method is computationally simpler to implement than autocorrelation analysis. For a series of Poisson events, as in the reactions modeled here, probability theory predicts that maximum likelihood for the series is the average value of the Poisson process (Matthews and Walker, 1964). Thus, a reasonable estimation of the real value results from measuring only a few cycles; however, autocorrelation analysis depends on the system being in a stationary state; therefore, measurement of only a limited number of cycles may not meet this requirement.

A graphical comparison of the two data analyses methods is shown in Figure 1.3 for simulated data sets of the same single molecule. Figure 1.3 clearly shows that as the

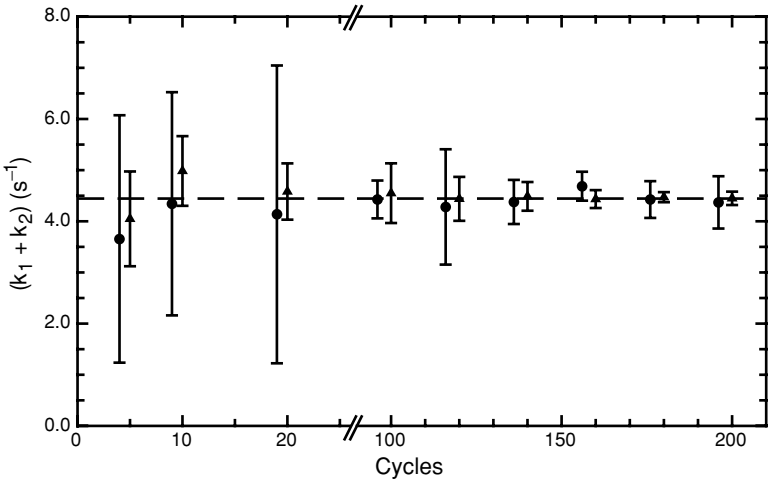

Figure 1.3. Comparison of the sum of the rate constants for a single molecule calculated either by autocorrelation analysis or averaging the "on and off" times for a given number of cycles as indicated on the x axis. For clarity, the points for the autocorrelation analysis are on one side of the points for the averaging method; the points for the averaging method give the true number of cycles for the other method. The circles (•) are the autocorrelation fit values and the triangles (▲) are the values determined by averaging for the rate constant sum. The error bars are the standard deviations for five independent simulations. The dashed horizontal line at 4.444 s^{-1} is from the parameters used in the simulation of the data stream in Table 1.1 and represents the true value.

number of cycles increases, both methods give similar values for the sum of the rate constants ($k_1 + k_2$). For example, at 150 cycles, the values are 4.58 ± 0.53 and 4.46 ± 0.19 for autocorrelation and averaging, respectively. However, for a limited number of cycles, generally less than 20, the accuracy of the averaging method is usually greater than that for autocorrelation analysis. For example, in Figure 1.3, the averaging method for the five cycles gives the sum of the rate constants within 10% of the true value, whereas autocorrelation analysis gives a value within 18%; in addition, the standard deviations of the simulations are greater for autocorrelation analysis.

Another possible advantage of the averaging method is the analysis of long-time data sets. A "moving" average, a nonweighted average over successive subsets of the data, which is commonly used in assembly line quality control, identifies any slow processes, such as conformation changes, occurring on a time scale long with respect to changes between states. Because the averaging method gives a reasonable result with between 5 and 15 measurements, a moving average can be applied to a subset within this range to determine where any changes are occurring. Once any changes are identified, the data can be reanalyzed by adjusting the subset size to give favorable results. Autocorrelation analysis of a system with slow conformation changes gives deviations from simple exponential decay; however, it may be difficult to determine when the deviations occurred. More complicated autocorrelation functions are needed to fit the deviations (Schenter et al., 1999; Yang and Xie, 2002b). To our knowledge, the use of a moving average method—a simple, powerful technique—to single molecule studies has not been reported previously.

Noise Considerations. The noise considerations for each type of analysis are quite different. The averaging method measures time widths whereas autocorrelation analysis measures

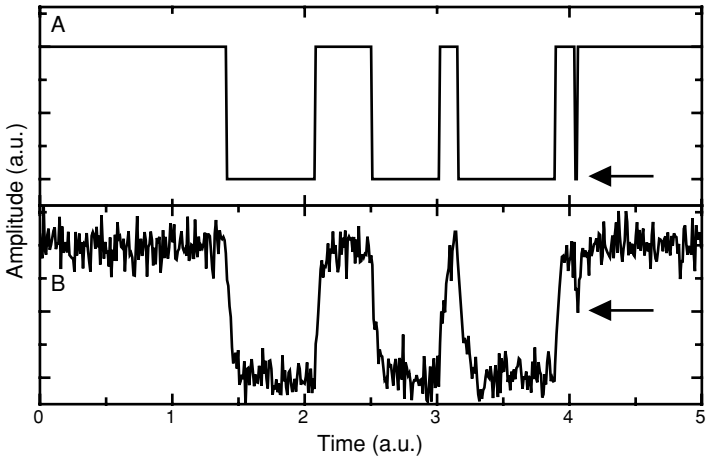

Figure 1.4. (A) Simulated data for an on and off process. (B) Identical data as in part A except noise and an RC constant of 0.04 time units are added; the amount of noise added gives a signal-to-noise ratio of approximately 5. Because the averaging method requires distinguishable states, the signal-to-noise ratio is important; a threshold amplitude value can be chosen to determine the molecule's state. If the noise level approaches the threshold value, discrimination between states is difficult. For example, in part B, if the threshold value for being in part A is set to greater than 0.5, then time spent in part B for a cycle, as indicated by the arrow, is overlooked. Alternatively, setting the threshold value to a smaller value can lead to noise signals interpreted as changes in state.

intensity fluctuations. Assuming a reasonable signal-to-noise ratio (i.e., the ability to distinguish states), the uncertainty for measurement of the widths of the on and off pulses depends largely on the RC constant of the detector and measurement system (see Figure 1.4). A large RC constant has the effect of noise reduction and data smoothing, but fast transitions between states are integrated and are potentially not resolvable. Because the autocorrelation function analyzes fluorescence intensity fluctuations as the molecule cycles between A and B, it is subject to shot noise associated with photon counting, white noise, $1/f$ noise, and other technical noise; however, most noise is uncorrelated, and thus there is a reduction of noise proportional to the square root of the number of time bins.

The method of choice for data analysis depends largely on the data itself:

1. If the signal-to-noise ratio is low (i.e., it is difficult to distinguish individual states), autocorrelation analysis is the preferred method.
2. If individual states are distinguishable and the amount of data is limited, then the averaging method generally yields more accurate results.
3. If individual states are distinguishable and the amount of data is not limited, then both the averaging method and autocorrelation analysis give equivalent results.

1.2.4.2. Prebulk Case

Both the averaging method and autocorrelation analysis assume that the chemical system is known in the probe volume. In addition to the former requirement, the averaging of the periods when all the molecules are either *all on* or *all off* involves knowledge of the molecular brightness if either individual rate constants or N is to be ascertained from the system. The

best type of analysis for the prebulk system, for two fluorescent states, is a combination of both methods. For this case, autocorrelation analysis gives $k_1 + k_2$, whereas the averaging method gives K_{eq}. By combining the results of both types of analysis, individual rate constants and N are determined. The noise considerations are analogous to those for the $N = 1$ case.

1.2.4.3. Bulk Case

In the bulk case, data analysis is limited to either the time dependence of the fluorescence intensity or autocorrelation analysis. Generally, for under 100 molecules, autocorrelation analysis is preferred because of its noise reduction feature. Because the relative intensity fluctuations become smaller as the number of molecules in the probe volume increases, autocorrelation analysis of bulk systems is not appropriate due to signal-to-noise considerations. Thus, time analysis of the relaxation following a perturbation jump experiment for bulk systems for large numbers of molecules may be the only method to determine the sum of the rate constants. In this case, technical noise is the main source of noise.

1.3. PROBE VOLUMES

In many interesting biological cases—for example, cells and lipid vesicles—choosing the probe volume is not possible. The determination of N is often the object of the experiment. In the previous section we discuss the treatment of data for multiple molecules in the probe volume. Here we examine the importance of the choice of a probe volume for single-molecule measurements and methods for attaining probe volumes smaller than can be obtained with diffraction optics.

The requirement that the average occupancy of the probe volume be less than one limits the range of reactions that can be studied by single-molecule studies (Laurence and Weiss, 2003). Consider the reaction

$$\mathrm{A} \underset{k_a}{\overset{k_d}{\rightleftharpoons}} \mathrm{A} + \mathrm{B} \tag{1.10a}$$

$$K_D = \frac{k_d}{k_a} = \frac{[\mathrm{A}][\mathrm{B}]}{[AB]}, \tag{1.10b}$$

where K_D is the equilibrium constant, k_a is the association rate constant, and k_d is the dissociation rate constant.

The magnitude of K_D is inversely related to the strength of the complex; K_D is often called the affinity to reflect this relationship. A small affinity value indicates a tightly bound complex. Here, affinity values of AB where the complex is half-dissociated are examined:

$$[\mathrm{B}] = [\mathrm{AB}] \tag{1.11a}$$

$$[B] = C_0/2 = K_D, \tag{1.11b}$$

where C_0 is the concentration corresponding to one analyte molecule in the probe volume. At equilibrium, k_d equals $(k_a \times C_0/2)$ and the recombination rate is $(k_a \times C_0/2)$. Assuming

Table 1.3. Representative Parameters for the Different Probe Volumes[a]

Method	Volume (fL)	C_0 (nM)	Dissociation Time (s)	Affinity (nM)
Focused flow	1.0×10^3	1.7×10^{-3}	1.2×10^4	8.3×10^{-4}
Droplets	1.0	1.7	12.1	0.8
Two-photon	1.0	1.7	12.1	0.8
Nanochannels	0.3	5.5	3.6	2.8
Confocal	0.2	8.3	2.4	4.2
TIR	0.1	16.6	1.2	8.3
TIR/FCS	5.0×10^{-2}	33.2	0.6	16.6
Two-plate	5.0×10^{-3}	3.3×10^2	0.1	1.7×10^2
Waveguide	1.0×10^{-6}	1.7×10^6	1.2×10^{-5}	8.3×10^5
Human cell	6.6×10^4	2.5×10^{-5}	1.6×10^6	1.3×10^{-5}

[a]Column 1 lists the method used to attain the probe volume listed in column 2. Column 3 lists the concentration, C_0, where there is, on average, one molecule in the probe volume. The dissociation time is the time needed for the complex to split—that is, the inverse of k_d. The affinity, K_D, is defined as the concentration where the complex is half-dissociated, [B] = [AB] , and the affinity is $C_0/2$.

that the forward reaction is diffusion controlled, k_a is approximately 10^8 $M^{-1} \cdot s^{-1}$ for a typical protein in water (Cantor and Schimmel, 1980).

A particular probe volume is appropriate for a limited range of affinities. For example, a volume of 0.2 fL, typically used in single-molecule confocal spectroscopy, requires a concentration less than 8.3 nM for an average occupancy of less than 1. This corresponds to an affinity of approximately 4 nM. It would be difficult to study molecules with larger affinities in this probe volume because the lower C_0 would result in unacceptable dissociation times resulting in fewer observable events. (See Table 1.3.) Two ways around this problem are smaller probe volumes and multiple occupancy of the probe volume.

Various ways of attaining probe volumes smaller than 1 fL are described below and are listed in Table 1.3; the volumes cover the range from picoliters to zeptoliters. This table illustrates several important points. Using the correct probe volume is critical when studying probe/target binding. While the range of affinities for a particular probe volume is limited, affinities from 10^{-3}–10^6 nM can be studied by choosing the appropriate probe volume.

It is mistakingly perceived that the diffraction of light limits the smallest probe volume to approximately a femtoliter (1 μm × 1μm × 1μm). Indeed, the most commonly used probe volume is 0.2 fL attained by diffraction limited, confocal optics. The most common way to exceed the limits imposed by diffraction optics is to use an evanescent field (Ambrose et al., 1999). When light strikes a transparent surface at an angle that exceeds the critical angle essentially all of the light is reflected, this effect is called total internal reflection (TIR). However, a small fraction of light "leaks" into the media; this is the evanescent wave. The intensity of the evanescent wave decreases exponentially with an e^{-1} length in the range of 100–500 nm. Probe volumes smaller than 1 fL are attained by a combination of confocal detection, spatial confinement into volumes with dimensions smaller than the wavelength of light, and evanescent excitation (Foquet et al., 2002; Ha et al., 1999; Hassler et al., 2005; He et al., 2005; Mukhopadhyay et al., 2004; Schwille; 2003; Starr and Thompson, 2001). TIR techniques are well-suited for studying single molecules at interfaces such as surfaces and cellular membranes (Schwille, 2003; Starr and Thompson, 2001). Foquet et al. (2002) reported a probe volume of 0.05 fL by confocal excitation of a sample confined between two

glass plates separated by 100 nm. Craighead's group recently combined spatial confinement and evanescent excitation; the sample was placed in a 200-nm inner-diameter quartz tube and excitation light was focused into the tube, resulting in an evanescent wave in the tube that gave a probe volume of 10^{-6} fL (Levene et al., 2003).

Two-photon excitation is another attractive way to define a small probe volume (Mertz et al., 1995). In two-photon spectroscopy, molecules are excited by the simultaneous absorption of two photons. Because the absorption is a two-photon process, the excitation probability is proportional to the square of the irradiance yielding probe volumes smaller than 1 fL (Schwille, 2001). Excitation of visible fluorophores is confined to the high irradiance region reducing both photobleaching of molecules outside of the probe volume and background luminescence from intracellular material.

1.4. STATISTICS OF SINGLE-MOLECULE MEASUREMENTS

1.4.1. Application to DNA Fingerprinting

This section describes our work on DNA fragment sizing (Ferris et al., 2005; Goodwin et al., 1993; Habbersett and Jett, 2004; Larson et al., 2000) that we include as a demonstration of the validity of extracting ensemble properties from less than ten molecules. Previously, we have measured the fluorescence intensity of individual DNA restriction fragments intercalated with a fluorescent dye to obtain a DNA fingerprint of a chromosome from a single bacterial cell or viral particle (Ferris et al., 2005). DNA intercalating dyes react stoichiometrically with DNA, resulting in a fluorescence signal that is proportional to the number of base pairs in the fragment. A histogram of the fluorescence intensity from individual restriction fragments is a DNA fingerprint.

1.4.1.1. Flow Cytometry

For analytical measurements, both an orderly delivery of analyte to the detection volume and efficient detection of analyte molecules are desired. One approach to this problem is detection in flowing sample streams. This method is based upon the use of hydrodynamic focusing to position sample streams in the center of a square-bore flow cell. When care is taken to ensure that the sample stream passes through the probe volume, such that all of the molecules experience similar excitation and optical detection efficiencies, the molecular detection efficiency is greater than 90% at a detection rate of approximately 100 molecules/s (Keller et al., 2002). Our flow approach to DNA sizing is roughly 100 times faster (from days to minutes), one million times more sensitive (from micrograms to femtograms), five times more certain (from 10% to 2%), and more accurate in the range of 125 bp to 450 kbp than gel electrophoresis (Larson et al., 2000). Figure 1.5 shows a DNA fingerprint from a *Hind*III digest of λ phage DNA (Habbersett and Jett, 2004). Fluorescence from approximately 1800 fragments is used to construct this histogram. How many were really needed?

Figure 1.6 illustrates how accurately the mean of a Gaussian distribution can be determined from the average of m measurements where $m = 2, 5, 10$, and 20 (Ferris et al., 2004). Only two measurements are required to reasonably estimate the mean and m greater than or equal to five does remarkably well for a Gaussian distribution. Figure 1.6 can be thought of as a graphical representation of the maximum likelihood theorem; that is, the most probable

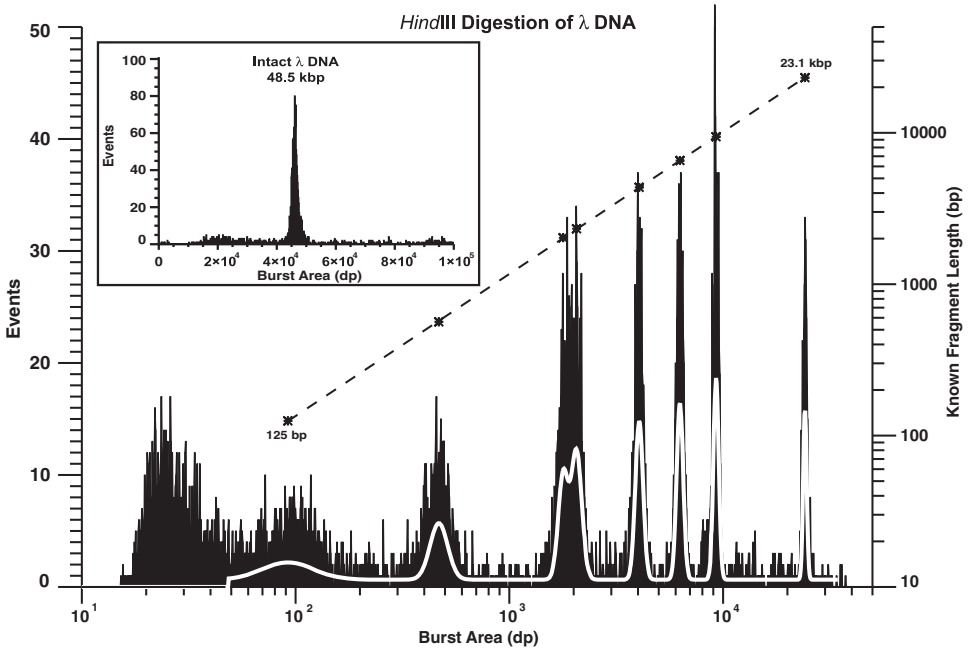

Figure 1.5. *Hind*III digest of λ phage DNA stained with SYTOX-orange and irradiated with 0.8 mW at 532 nm from continuous Nd:YAG laser. The *y* axis is the number of events, and the *x* axis is the burst area in detected photons. The histogram is constructed from a total of 1800 events recorded in 124 s from a 1–10 pM solution of fragments. The white curve is the sum of eight Gaussian distributions fit to the data; the amplitude of the curve is drawn at half-scale for visibility. The dashed line is a plot of the Gaussian centroids versus the known fragment lengths. The inset is a histogram of intact λ phage DNA with a CV of 1.6% on the major peak. [Reprinted from Habbersett and Jett (2004), with permission of Wiley-Liss.]

outcome for a random sequence of numbers from a Gaussian distribution is the average value of the distribution (Matthews and Walker, 1964).

Figure 1.7 shows the effect of reducing the sample size in an *S. aureus* restriction digest assay from 14,163 fragments to 570 fragments (Ferris et al., 2004). The sample size of 570 ensures that there are at least 10 replicate measurements of each fragment. The smaller-sized sample results in a loss of resolution, but still gives a representative fingerprint.

1.4.1.2. Optical Mapping

We use optical mapping techniques developed by David Schwartz and colleagues (Aston et al., 1999; Meng et al., 1995; Schwartz et al., 1993; Schwartz and Samad, 1997) to obtain DNA fingerprints from single viral genomes deposited on a surface (Ferris et al., 2005). Briefly, the experimental procedure involves embedding cells in an agarose matrix, lysing the cells, and processing to yield intact DNA. The DNA is then deposited on a derivatized glass substrate, which stretches out the genome. The elongated genome is digested with a restriction enzyme and stained with YOYO-1, an intercalating dye. The DNA relaxes upon cutting, leaving gaps at the restriction sites and intact DNA between restriction sites; after digestion, the order of the fragments is preserved. We use a concentration of 25 ng/mL

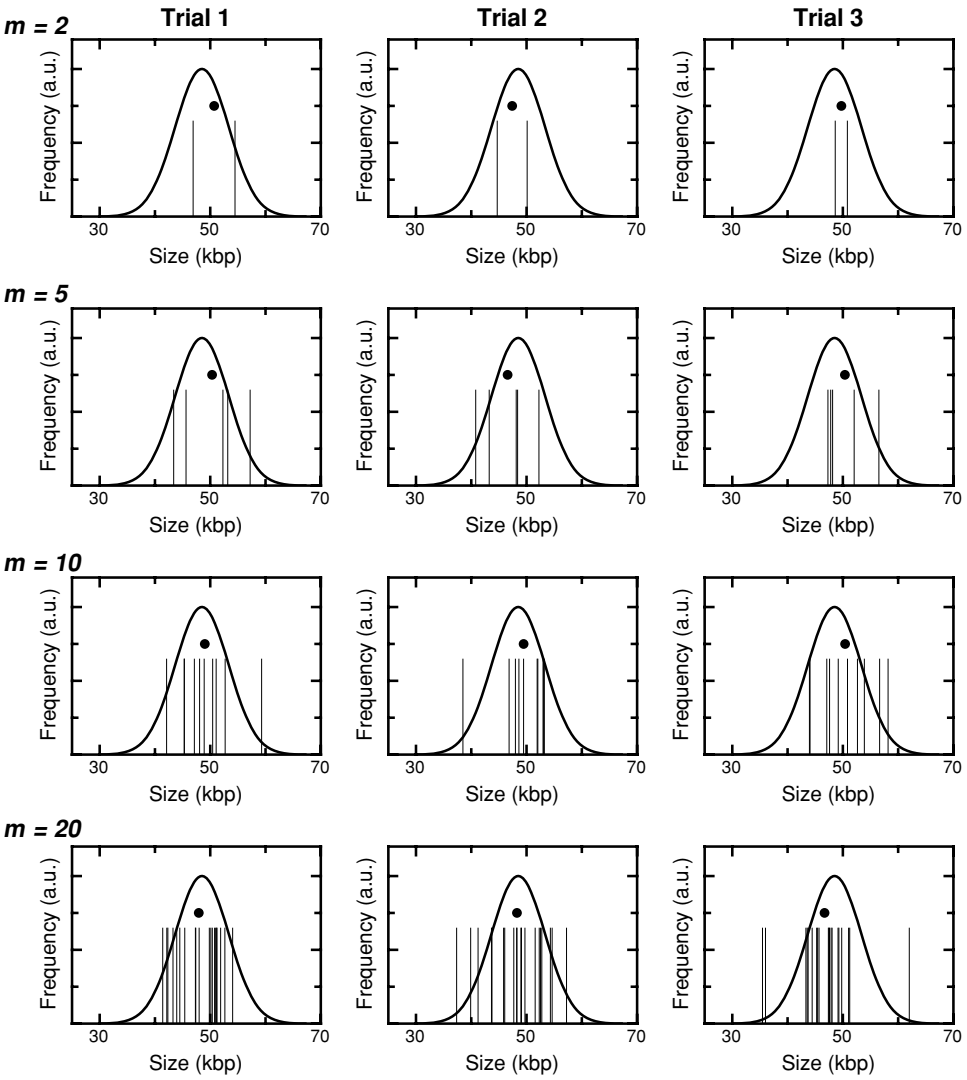

Figure 1.6. Distribution of randomly chosen single molecules within a Gaussian profile representative of an intact λ phage DNA fragment generated using a mean of 48.502 kbp and a CV of 10%. The solid curve represents the Gaussian distribution whereas the vertical lines denote the positions of the random picks and the filled circle denotes the average of the *m* picks. [Reprinted from Ferris et al. (2004), with permission of Wiley-Liss.]

of intact viral genomes to obtain one genome per 10^4 μm^2. Fluorescence from individual fragments is collected with a CCD camera mounted on a sensitive microscope.

Figure 1.8 shows fluorescence from a *Pme*I digest of a mixture of λ phage and bacteriophage T4, strain GT7. The fragment patterns are clearly different and easily distinguished from each other. We use the known sizes of T4 GT7 restriction fragments and a CV of 8%, characteristic of our measurements, to construct a virtual fingerprint of T4 GT7. DNA fragment lengths measured from seven T4 GT7 genomes, using λ phage DNA as an intensity standard, are plotted in Figure 1.8. Fragments from individual genomes are identified

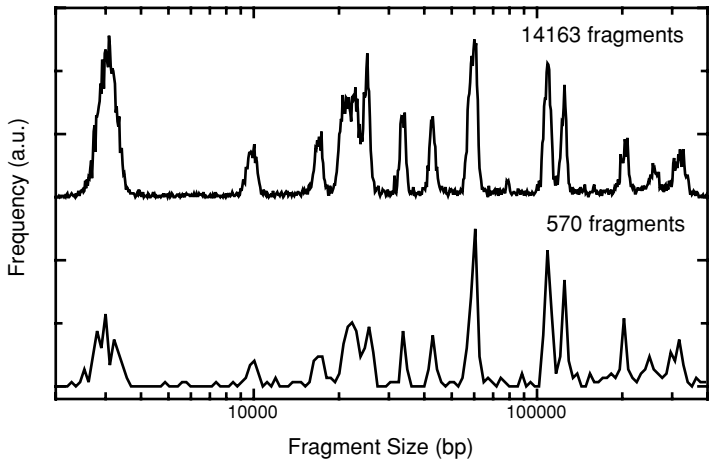

Figure 1.7. Comparison of the DNA fragment size distribution from a *S. aureus* Mu50 digested with *Sma*I derived from the measurement of 14000 fragments to a distribution derived from a measurement of 570 fragments. [Reprinted from Ferris et al. (2004), with permission of Wiley-Liss.]

by a color code. The fragment lengths from the individual cells are closely grouped, and a fingerprint from any one of the seven genomes represents the actual fingerprint.

Figure 1.9A shows a fluorescence image from a *Pme*I digest of a mixture of adenovirus, λ phage, and T4 GT7. Again the fingerprints are easily identified by their pattern. Figure 1.9B shows the fragment lengths measured in Figure 1.9A plotted on top of a virtual digest of adenovirus and T4 GT7. The λ digest is used to calibrate the fragment sizes. These data show that optical mapping techniques can identify the composition from a mixed sample. This is in contrast to restriction fragments analyzed by either gel electrophoresis or flow

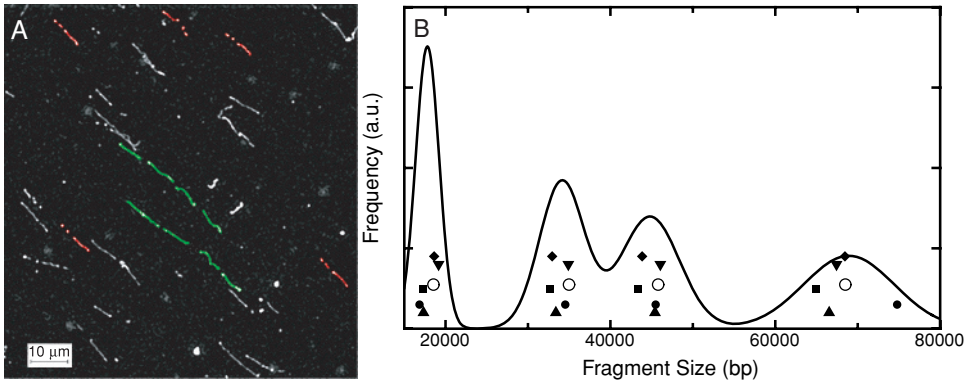

Figure 1.8. (A) A portion of a fluorescence image displaying stained DNA fragments of a *Pme*I digest of a mixture of λ phage DNA, falsely colored red, and T4 GT7, falsely colored green. The different genomes are easily identified by their respective patterns. See insert for color representation of figure A. (B) Seven distinct T4 GT7 genomes from the complete image shown in part A plotted on top of a virtual digest of T4 GT7. The data are offset from each other on the *y* axis for viewing. The two T4 GT7 genomes in part A are denoted by the square (■) and the open circle (O) in the plot. The fluorescence intensity of the T4 GT7 genomes is calibrated with data from the λ phage DNA. [Reprinted from Ferris et al. (2005), with permission of Elsevier.]

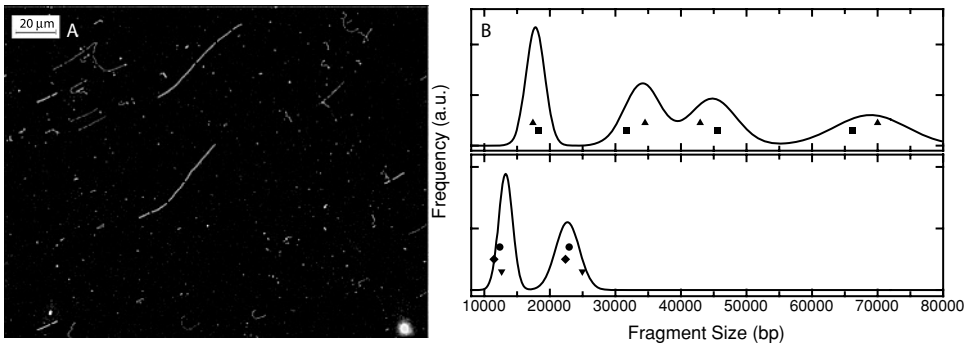

Figure 1.9. (A) *Pme*I digestion products of a mixture containing adenovirus (three genomes in blue), λ phage DNA (three genomes in red), and T4 GT7 DNA (two genomes in green). See insert for color representation of figure A. (B) Fragment sizes of T4 GT7 and adenovirus from part A are plotted on a virtual digests of the components using an 8% coefficient of variation. The lower plot in part B is adenovirus, whereas the upper plot is T4 GT7. [Reprinted from Ferris et al. (2005), with permission of Elsevier.]

cytometry that pass through a solution phase where fragment order is lost and therefore cannot be related to the species of origin.

Knowing the order of the restriction fragments on the genome provides another dimension in DNA fingerprinting that is a significant advantage when discriminating between two organisms or when matching the fingerprint of an unknown organism to a library entry. There are $N!$ ways of arranging N restriction fragments on a chromosome. Electrophoresis and flow cytometry provide a histogram of the fragment sizes but not the order of the fragments. This means there are $N!$ potential matches to other organisms in an electrophoretic or flow assay whereas an ordered map has only one match.

This point is illustrated in Figure 1.10A for the fingerprint of a pair of hypothetical genomes that contain three restriction fragments with two degenerate fragments. We have developed a "bingo card" display that incorporates both the fragment size and the fragment order to remove the degenerancy. The x axis reports the size of the restriction fragments, and the y axis indicates the order of the fragments.

1.5. VIRTUAL SORTING

It is difficult to sort single molecules by conventional flow cytometric techniques because the flow rates are too slow. Kapanidis et al. (2004) use fluorescence resonance energy transfer, herein referred to as FRET, to select emission from donor/acceptor-labeled biomolecules for "virtual sorting." In virtual sorting, the data stream is sorted instead of the sample stream. Consider the gedanken experiment shown in Figure 1.11. The sample contains four components: free dye, unlabeled target, labeled probe, and probe/target complex. One is interested in measuring the ratio of the number of bound and unbound probes containing a single tag. The chemistry is complex, and it is difficult to separate chemically free dye and probes containing more than one fluorescent tag from the solution. This can be important for analyses involving complex labeling schemes. (See Section 1.6.)

Theoretical data from a mixture of the three components is shown in Figure 1.11. The three components have different molecular weights and therefore different diffusion constants; consequently, they spend different times in the probe volume. The "sorter" directs the

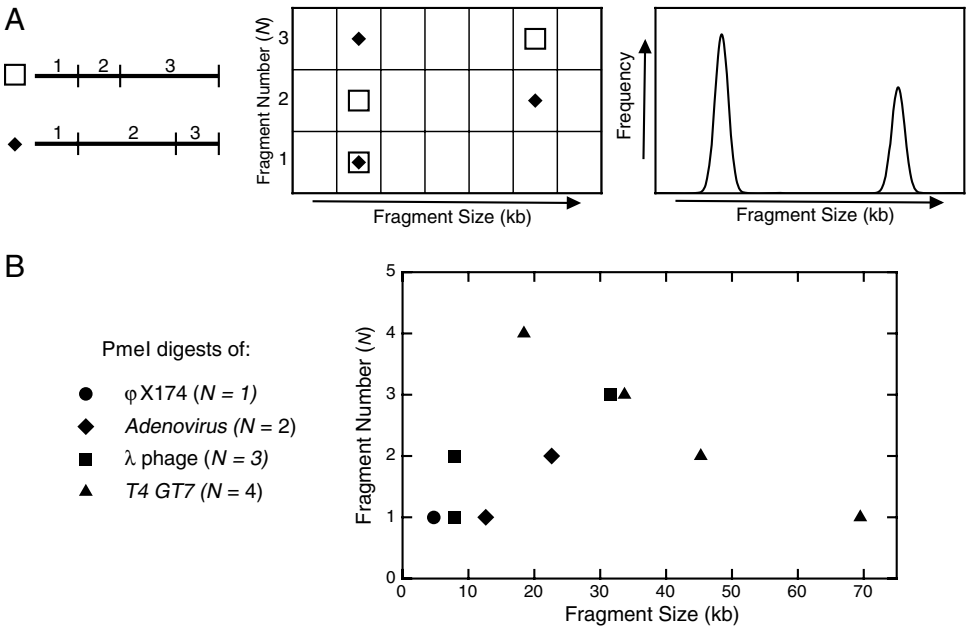

Figure 1.10. (A) A hypothetical example of a bingo card display for two different genomes; the two genomes are denoted by the open rectangle (□) and the filled diamond (⧫). Both genomes contain identical fragments but with a different distribution. The middle of part A shows a bingo card display where each genome is distinguishable, whereas the rightmost plot in part A shows a histogram of the fragment sizes analogous to those from gel electrophoresis or flow cytometry. In the rightmost plot the fragments from the individual genomes are mixed together, eliminating the possibility of distinguishing between genomes. (B) Bingo card display for the genomes digested with *Pme*I in Figures 1.8 and 1.9. Fragments 1 and 2 of the λ digest, normally undetermined by gel electrophoresis and flow cytometry, are clearly visible in the bingo card presentation. [Reprinted from Ferris et al. (2005), with permission of Elsevier.]

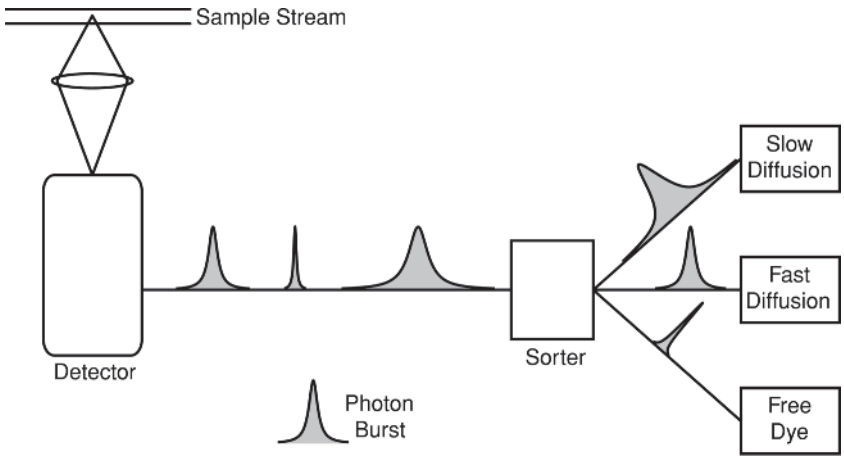

Figure 1.11. Schematic of an apparatus for sorting the data stream into bins corresponding to the molecule in the probe volume—that is, virtual sorting. The molecules are identified by their diffusion time, which is reflected by the length of the photon burst as the molecule diffuses through the probe volume.

data from the different species into the appropriate data bin. Hence, the ratio of the bound to unbound probes is obtained *without* ever purifying the mixture. Similar techniques can be used to determine FRET efficiencies without separating species containing only a donor or acceptor from the mixture.

1.6. STATISTICAL CHEMISTRY

Statistical chemistry is a new way of doing chemistry that would be a good application for virtual sorting. Figure 1.12 shows a synthetic pathway for the preparation of a molecule containing a FRET donor/acceptor pair for the study of conformation changes of large polymer molecules (e.g., proteins or DNA). Typically, two different reactive groups are added to the analyte (e.g., amine and carboxyl), and the donor and acceptor tags contain the appropriate complementary reactive groups. Consider Reaction A in Figure 1.12, which shows a labeling reaction for a protein with a donor and acceptor pair for a FRET experiment. DPA, which contains a single donor and acceptor, is the desired product; the other species are byproducts that contribute to the fluorescence background and perturb the answer. The amount of the various byproducts depends upon the selectivity of the reactive groups and the reaction conditions. Extensive column chromatography and other purification techniques can remove byproducts (i.e., unbound dyes) with only limited success. In fact, much of the data in the literature contain artifacts from byproducts. The autocorrelation function can show the presence of unwanted contaminants. For example, the presence of unreacted donors or acceptors would show up in the autocorrelation function as species with large diffusion coefficients.

A more challenging situation is where both reactive groups are identical—for example, either amine or carboxyl. In this case, virtual sorting can be a real aid. Consider Reaction B in Figure 1.12, where P has two reactive amines and both donors and acceptors contain a reactive SH group; both D and A are present at the same concentration. Again, the desired product is DPA, statistically 50% of the reaction yield. Extraction of these compounds from the reaction mixture by chromatography is exceedingly difficult, but separation of the data stream by selecting species that emit in both the red and green or emit in the red when excited in the green is relatively straightforward.

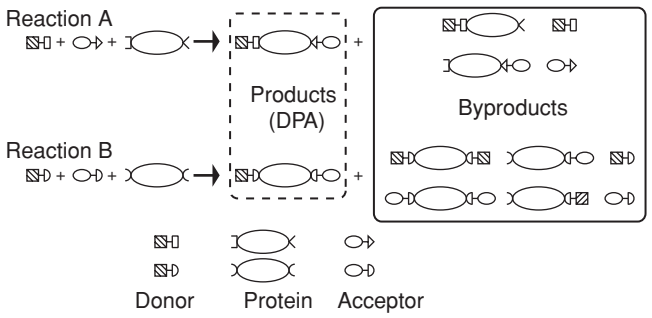

Figure 1.12. Reaction A is a donor/acceptor reaction for a protein with different binding sites for donor and acceptor. The desired product, DPA, is marked by a dashed rectangle, whereas the byproducts of the reaction (i.e., incompletely labeled protein, incorrectly labeled protein, and free dye) are marked by the solid rectangle. Reaction B is a donor/acceptor reaction for a protein with identical binding sites for donor and acceptor. The desired products and byproducts are denoted with a dashed and solid line rectangle, respectively.

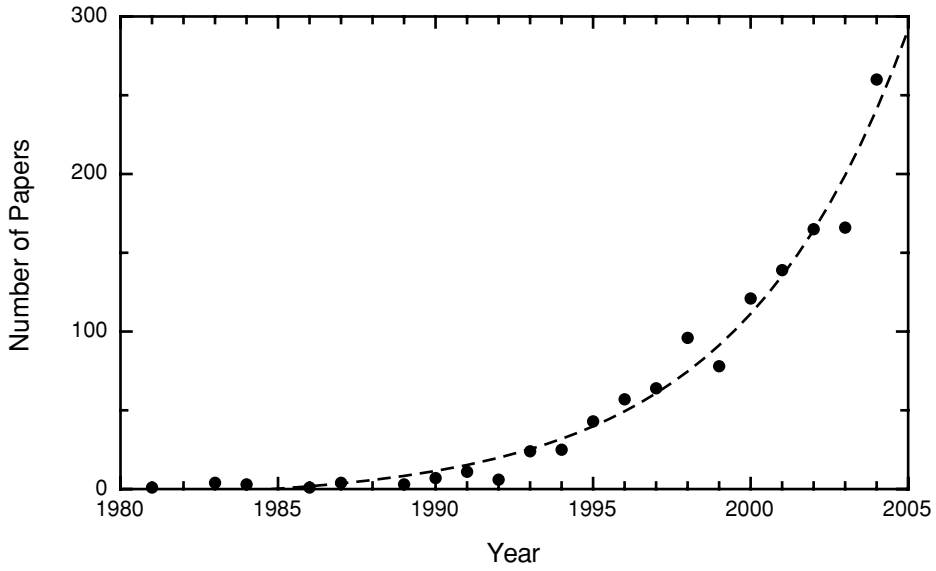

Figure 1.13. The approximate number of papers published concerning single-molecule studies; the number of papers doubles every three years. The dashed line is drawn only to indicate the trend. The number of papers published is found with SearchPlus^{TM}, a literature database.

1.7. THE FUTURE

It is appropriate to begin a discussion of the future with a brief summary of the past. Considerable progress has been made in analytic detection of organic molecules over the last 25 years. In 1983 the world record for the detection of fluorescent molecules in solution was 22,000 molecules in a 10-pL probe volume (Dovichi et al., 1983); in 1990, single-molecule detection in flow was achieved (Goodwin et al., 1995). Since 1990, the number of papers in single-molecule research has grown exponentially with no signs of a slowdown. Figure 1.13 shows a growth curve for single-molecule publications which indicates a promising future.

Currently, the majority of single-molecule research relies on fluorescence detection. In the near future, other intrinsic properties such as Raman spectra, absorption spectra, electrical properties, magnetic properties, and so on, will be increasingly used to characterize single molecules.

1.7.1. Medical Diagnostics

An area where single-molecule studies have great potential is medical diagnostics. Increasingly, modern medicine is becoming molecular medicine; diagnostics are beginning to be based upon single-molecule probe/target binding (e.g., antibody antigen). These diagnostics will become more important as probes become more selective, versatile, photostable, soluble, and compatible with intracellular environments. Indeed, one may even imagine mobile probes circulating through the body monitoring important functions and surveying for early indicators of a developing disease; these probes would broadcast reports to external receivers.

1.7.2. Single-Cell Chemistry and Biology

The ability to perform intracellular measurements for identification of species present, interaction between species, or tracking of species in response to stimulation is an emerging field in single-molecule detection. Future advancements will lead to a new understanding of basic biological processes in cells. Such information is not available from *in vitro* measurements. In fact, *in vitro* measurements are misleading because the pristine environment excludes interactions with surfaces and other cellular components that are important aspects of intracellular chemistry. A good starting point would be the encapsulation of selective intracellular species into lipid vesicles to mimic cells.

1.7.3. Sample Preparation and Detection

We expect a tremendous improvement in the handling of ultrasmall samples. One can detect single molecules, but it requires nanograms of sample to get a few molecules to the probe volume. New advances in nanotechnology permit handling of minute samples and delivery of such samples to an interrogation region.

1.7.3.1. Lab on a Chip

There is considerable activity in designing, constructing, and characterizing microfluidic devices of nanometer dimensions ("nanotechnology") for delivery of samples to small reaction chambers for the study of monomolecular and bimolecular chemistry of single species (e.g., single molecules, single DNA fragments, single cells, etc.). These devices incorporate valves, mixers, pumps, and detectors to form an integrated analysis system for nanochemistry—that is, a "*Lab on a Chip*."

In 2001, Chabinyc, Chiu, McDonald, Stroock, Christian, Karger, and Whitesides made considerable progress toward a total lab on a chip (Chabinyc et al., 2001). The chip incorporated a μAPD array, a fluidic system with a dedicated excitation/detection region, and fiber optics to deliver the excitation beam. The device had a detection sensitivity 25 nM fluorescein; future development will improve on the sensitivity.

Zare's group has developed a microfluidic device to study the reactions of single cells (Gao et al., 2004; Wheeler et al., 2003; Wu et al., 2004). The chip is constructed of soft polymethylsiloxane, has a reaction volume of 70 pL, and contains a metering system that can deliver picoliter volumes. In addition to ultrasensitive fluorescence detection, the device has an electrophoresis column and a fluidic trap incorporated into the chip. Briefly, samples are injected into a microchannel and a particular cell is selected and trapped in the reaction chamber. The cell is lysed and intracellular substances are released into the reaction chamber, where they combine with reagents introduced into the chamber. The products are then detected and characterized. In addition to a significant saving in time and reagents, intercellular heterogeneities are observed that would be obscured in the averaging that occurs in bulk measurements.

We anticipate a microchip incorporating many channels, where each channel contains (a) diode emitters for fluorescence excitation at a wavelength chosen by the operator, (b) pumps and valves for sample delivery, (c) an integrated single-molecule detector, (d) the ability to manipulate individual molecules, (e) a data processor, and (f) automated reporting.

1.7.3.2. Sample Preparation and Detection of Single Molecules on a Surface or in a Thin Layer of Agarose

By far, the easiest and most straightforward way to handle small samples is deposition on a surface or in a thin agarose gel (Ferris et al., 2005). Deposition on a surface minimizes sampling handling, allowing fragile samples to stay intact. In addition, it maintains spatial separation of the molecules in the sample, and thus any chemistry performed on the sample preserves this separation. Surface deposition analysis can easily be incorporated for automated analysis. We believe that surface deposition analysis will become a universal technique for single-molecule detection.

1.7.3.3. Analysis Rate

In order for single-molecule measurements to become a practical analytical tool, considerable improvement must be made in the analysis rate, currently 100 molecules/s. Capillary arrays are one approach that is being developed to increase the analysis rate. Currently, capillary arrays are used for DNA sequencing (Huang et al., 1992; Lu and Yeung, 1999; Mathies and Huang, 1992; Xue et al., 1999; Zagursky and McCormick, 1990; Zhang et al., 1999). However, capillary array detection is generally limited by a low duty cycle. We envision capillary arrays bundles becoming larger, having a larger throughput, increased sensitivity, and hyper-dimensional analysis. In fact, Dovichi has demonstrated two-dimensional analysis for DNA sequencing (Zhang et al., 2001).

1.7.3.4. Counting Individual Molecules and Sorting

Single-molecule detection and counting represent ultimate goals of analytical chemistry. If the signal from each molecule is observable, the molecular count rate is a digital process and directly measures the concentration. Current single-molecule detection efficiencies are between 80% and 90% (Goodwin et al., 1995; Lermer et al., 1997; Li and Davis, 1995; Zander et al., 1998), which will without doubt improve. In addition, probe volumes will become larger, allowing more sample to be analyzed at the same time.

Sorting techniques for detected and identified single molecules will be improved. This will enable separation and concentration of selected (rare) species from a heterogeneous sample for reanalysis, cloning, or further study. Reanalysis could involve increasing the accuracy/confidence of the initial analysis or identifying sorted species that contain another parameter (e.g., all DNA fragments of a given size that contain a specific sequence). Single-molecule manipulation techniques will enable selective chemical reactions and molecular assembly.

1.7.4. Simplified Apparatus or a Poor Man's Single-Molecule Detector

Presently, single-molecule detection, which includes the detection equipment, electronics, and light sources, occupies a substantial portion of a laboratory. We foresee a day where apparatus is less in both size and cost. "Off-the-shelf" components will be used to construct such apparatus. Single-molecule detectors will be come as commonplace as typical instruments in any analytical laboratory (see Figure 1.14) and will be found in medical, diagnostic, and analytical laboratories.

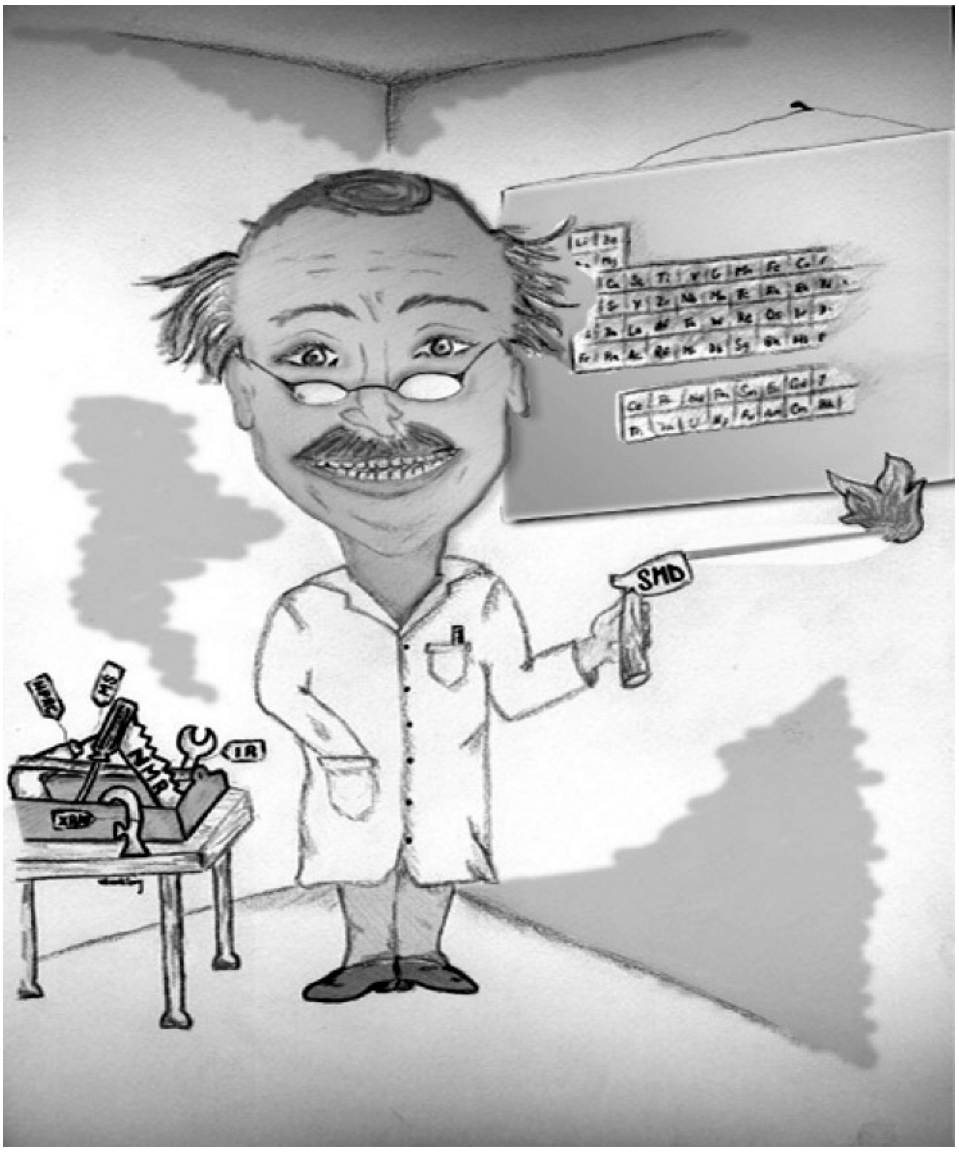

Figure 1.14. Single-molecule detection is becoming just "another tool" in an experimentalist's toolbox.

1.8. CONCLUSIONS

We constructed a model system for single and multiple molecules in a probe volume. We used simulated data to explore various methods of analysis: autocorrelation, averaging, and distribution analyses. Each method of analysis has its strengths and weaknesses; the most prudent method of analysis is often a combination of the various techniques to complement each other. Single-molecule properties (i.e., k and K_{eq}) can be extracted when there is no more than 10 molecules in the probe volume; synchronous starts are not necessary for this type of system.

Section 1.3 discusses the relationship between probe volumes and affinities for particular reaction kinetics. Insight to the reaction kinetics is helpful before beginning a single-molecule experiment to determine the "best" probe volume for a mechanism.

New methods of analysis can often simply experimental procedures. Statistical chemistry and virtual sorting can be used to analyze properties of selected molecules from a complex mixture without chemical separation and purification.

Lastly, the answer to our initial question, "Is one enough?" For accurate measurements, the answer is most likely *no*. However, we show that as few as two measurements are needed (see Figure 1.9); generally, 10–14 measurements are typically more than sufficient.

ACKNOWLEDGMENTS

We have been fortunate in having quality postdocs and colleagues, who have been largely responsible for our success. We thank the Department of Energy for 25 years of continued support. We also acknowledge the support of the NIH/NCRR funded National Flow Cytometry Resource, Grant RR-01315. Special thanks to Lawrence Pratt for informative discussions about data handling and subtleties in the statistics when studying the properties of a small number of molecules confined to a small volume.

REFERENCES

Ambrose, WP, Goodwin, PM, and Nolan, JP (1999). Single-molecule detection with total internal reflection excitation: Comparing signal-to-background and total signals in different geometries. *Cytometry B Clin Cytom* **36**:224–231.

Aragon, SR, and Pecora, R (1976). Fluorescence correlation spectroscopy as a probe of molecular dynamics. *J Chem Phys* **64**:1791–1803.

Aston, C, Mishra, B, and Schwartz, DC (1999). Optical mapping and its potential for large-scale sequencing projects. *Trends in Biotechnol* **17**:297–302.

Baldini, G, Cannone, F, and Chirico, G (2005). Pre-unfolding resonant oscillations of single green fluorescent protein molecules. *Science* **309**:1096–1100.

Cantor, CR, and Schimmel, PR (1980). *Biophysical Chemistry III: The Behavior of Biological Macromolecules*. Freeman, New York.

Chabinyc, ML, Chiu, DT, McDonald, JC, Stroock, AD, Christian, JF, Karger, AM, and Whitesides, GM (2001). An integrated fluorescence detection system in poly(dimethylsiloxane) for microfluidic applications. *Anal Chem* **73**:4491–4498.

Demas, JN (1983). *Excited State Lifetime Measurements*. Academic Press, New York.

Dovichi, NJ, Martin, JC, Jett, JH, and Keller, RA (1983). Attogram detection limit for aqueous dye samples by laser-induced fluorescence. *Science* **219**:845–847.

Elson, EL (1985). Fluorescence correlation spectroscopy, and photobleaching recovery. *Annu Rev Phys Chem* **36**:379–406.

Ferris, MM, Habbersett, RC, Wolinsky, M, Jett, JH, Yoshida, TM, and Keller, RA (2004). Statistics of single-molecule measurements: Applications in flow-cytometry sizing of DNA fragments. *Cytometry B Clin Cytom* **60A**:41–52.

Ferris, MM, Yoshida, TM, Marrone, BL, and Keller, RA (2005). Fingerprinting of single viral genomes. *Anal Biochem* **337**:278–288.

Foquet, M, Korlach, J, Zipfel, W, Webb, WW, and Craighead, HG (2002). DNA fragment sizing by

single molecule detection in submicrometer-sized closed fluidic channels. *Anal Chem* **74**:1415–1422.

Gao, J, Yin, XF, and Fang, ZL (2004). Integration of single cell injection, cell lysis, separation and detection of intracellular constituents on a microfluidic chip. *Lab on a Chip* **4**:47–52.

Goodwin, PM, Wilkerson, CW, Ambrose, WP, and Keller, RA (1993). Ultrasensitive detection of single molecules in flowing sample streams by laser-induced fluorescence. *"Proc SPIE–Int Soc Opt Eng* **1895**:79–89.

Goodwin, PM, Affleck, RL, Ambrose, WP, Demas, JN, Jett, JH, Martin, JC, Reha-Krantz, LJ, Semin, DJ, Schecker, JA, Wu, M, and Keller, RA (1995). Progress toward DNA sequencing at the single molecule level. *Exp Tech Phys* **41**:279–294.

Ha, T, Laurence, TA, Chemla, DS, and Weiss, S (1999). Polarization spectroscopy of single fluorescent molecules. *J Phys Chem B* **103**:6839–6850.

Habbersett, RC, and Jett, JH (2004). An analytical system based on a compact flow cytometer for DNA fragment sizing and single-molecule detection. *Cytometry B Clin Cytom* **60A**:125–134.

Hassler, K, Anhut, T, Rigler, R, Gosch, M, and Lasser, T (2005). High count rates with total internal reflection fluorescence correlation spectroscopy. *Biophys J* **88**:L1–L3.

He, MY, Edgar, JS, Jeffries, GDM, Lorenz, RM, Shelby, JP, and Chiu, DT (2005). Selective encapsulation of single cells and subcellular organelles into picoliter- and femtoliter-volume droplets. *Anal Chem* **77**:1539–1544.

Hill, TL (1960). *Introduction to Statistical Thermodynamics*. Addison-Wesley, Reading, MA.

Huang, XC, Quesada, MA, and Mathies, RA (1992). DNA sequencing using capillary array electrophoresis. *Anal Chem* **64**:2148–2154.

Jia, YW, Talaga, DS, Lau, WL, Lu, HSM, DeGrado, WF, and Hochstrasser, RM (1999). Folding dynamics of single GCN4 peptides by fluorescence resonant energy transfer confocal microscopy. *Chem Phys* **247**:69–83.

Kapanidis, AN, Lee, NK, Laurence, TA, Doose, S, Margeat, EE, and Weiss SS (2004). Fluorescence-aided molecule sorting: analysis of structure and interactions by alternating-laser excitation of single molecules. *Proc Natl Acad Sci USA* **101**:8936–8941.

Keller, RA, Ambrose, WP, Arias, AA, Cai, H, Emory, SR, Goodwin, PM, and Jett, JH (2002). Analytical applications of single-molecule detection. *Anal Chem* **74**:316A–324A.

Krichevsky, O, and Bonnet, G (2002). Fluorescence correlation spectroscopy: The technique and its applications. *Rep Prog Phys* **65**:251–297.

Larson, E, Hakovirta, J, Cai, H, Jett, JH, Burde, S, Keller, RA, and Marrone, BL (2000). Rapid DNA fingerprinting of pathogens by flow cytometry. *Cytometry B Clin Cytom* **41**:203–208.

Laurence, TA, and Weiss, S (2003). How to detect weak pairs. *Science* **299**:667–668.

Leadbetter, JR (2003). Cultivation of recalcitrant microbes: Cells are alive, well and revealing their secrets in the 21st century laboratory. *Curr Opin Microbiol* **6**:274–281.

Lermer, N, Barnes, MD, Kung, CY, Whitten, WB, and Ramsey, JM (1997). High efficiency molecular counting in solution: Single-molecule detection in electrodynamically focused microdroplet streams. *Anal Chem* **69**:2115–2121.

Levene, MJ, Korlach, J, Turner, SW, Foquet, M, Craighead, HG, and Webb, WW (2003). Zero-mode waveguides for single-molecule analysis at high concentrations. *Science* **299**:682–686.

Li, LQ, and Davis, LM (1995). Rapid and efficient detection of single chromophore molecules in aqueous solution. *Appl Opt* **34**:3208–3217.

Lu, S, and Yeung, E (1999). Side-entry excitation and detection of square capillary array electrophoresis for DNA sequencing. *J Chromatogr* **853**:359–369.

Mathies, RA, and Huang, XC (1992). Capillary array electrophoresis—an approach to high-speed, high-throughput DNA sequencing. *Nature* **359**:167–169.

Matthews, J, and Walker, RL (1964). *Mathematical Methods of Physics*, 2nd edition. Addison-Wesley, New York.

Meng, X, Benson, K, Chada, K, Huff, EJ, and Schwartz, DC (1995). Optical mapping of lambda bacteriophage clones using restriction endonucleases. *Nat Genet* **9**:432–438.

Mertz, J, Xu C, and Webb, WW (1995). Single-molecule detection by two-photon-excited fluorescence. *Opt Lett* **20**:2532–2534.

Mukhopadhyay, A, Bae, SC, Zhao, J, and Granick, S (2004). How confined lubricants diffuse during shear. *Phys Rev Lett* **93**:236105–236114.

Park, M, Kim, HH, Kim, D, and Song, NW (2005). Counting the number of fluorophores labeled in biomolecules by observing the fluorescence-intensity transient of a single molecule. *Bull Chem Soc Jpn* **78**:1612–1618.

Pennisi, EE (2004). The biology of genomes meeting. Surveys reveal vast numbers of genes. *Science* **304**:1591–1591.

Rhoades, E, Gussakovsky, E, and Haran, G (2003). Watching proteins fold one molecule at a time. *Proc Natl Acad Sci USA* **100**:3197–3202.

Riley, KF, Hobson, MP, and Bence, SJ (1997). *Mathematical Methods for Physics and Engineering*. Cambridge University Press, Cambridge, UK.

Schenter, GK, Lu, HP, and Xie, XS (1999). Statistical analyses and theoretical models of single-molecule enzymatic dynamics. *J Phys Chem A* **103**:10477–10488.

Schwartz, DC, Li, X, Hernandez, LI, Ramnarain, SP, Huff, EJ, and Wang, YK (1993). Ordered restriction maps of *Saccharomyces cerevisiae* chromosomes constructed by optical mapping. *Science* **262**:110–114.

Schwartz, DC, and Samad, A (1997). Optical mapping approaches to molecular genomics. *Curr Opin Biotech* **8**:70–74.

Schwille, P (2001). Fluorescence correlation spectroscopy and its potential for intracellular applications. *Cell Biochem Biophys* **34**:383–408.

Schwille, P (2003). TIR-FCS: Staying on the surface can sometimes be better. *Biophys J* **85**:2783–2784.

Soper, SA, Nutter, HL, Keller, RA, Davis, LM, and Shera, EB (1993). The photophysical constants of several fluorescent dyes pertaining to ultrasensitive fluorescence spectroscopy. *Photochem Photobiol* **57**:972–977.

Starr, TE, and Thompson, NL (2001). Total internal reflection with fluorescence correlation spectroscopy: Combined surface reaction and solution diffusion. *Biophys J* **80**:1575–1584.

Talaga, DS, Lau, WL, Roder, H, Tang, JY, Jia, YW, DeGrado, WF, and Hochstrasser, RM (2000). Dynamics and folding of single two-stranded coiled-coil peptides studied by fluorescent energy transfer confocal microscopy. *Proc Natl Acad Sci USA* **97**:13021–13026.

Vazquez, MI, Rivas, G, Cregut, D, Serrano, L, and Esteban, M (1998). The vaccinia virus 14-kilodalton (a27l) fusion protein forms a triple coiled-coil structure and interacts with the 21-kilodalton (a17l) virus membrane protein through a c-terminal alpha-helix. *J Virol* **72**:10126–10137.

Verberk, R, and Orrit, M (2003). Photon statistics in the fluorescence of single molecules and nanocrystals: Correlation functions versus distributions of on- and off-times. *J Chem Phys* **119**:2214–2222.

Wheeler, AR, Throndset, WR, Whelan, RJ, Leach, AM, Zare, RN, Liao, YH, Farrell, K, Manger, ID, and Daridon, A (2003). Microfluidic device for single-cell analysis. *Anal Chem* **75**:3581–3586.

Wu, HK, Wheeler, A, and Zare, RN (2004). Chemical cytometry on a picoliter-scale integrated microfluidic chip. *Proc Natl Acad Sci USA* **101**:12809–12813.

Xue, G, Pang, HM, and Yeung, ES (1999). Multiplexed capillary zone electrophoresis and micellar electrokinetic chromatography with internal standardization. *Anal Chem* **71**:2642–2649.

Yang, H, and Xie, XS (2002a). Statistical approaches for probing single-molecule dynamics photon-by-photon. *Chem Phys* **284**:423–437.

Yang, H, and Xie, XS (2002b). Probing single-molecule dynamics photon by photon. *J Chem Phys* **117**:10965–10979.

Yang, SL, and Cao, JS (2001). Two-event echos in single-molecule kinetics: A signature of conformational fluctuations. *J Phys Chem B* **105**:6536–6549.

Zagursky, RJ, and McCormick, RM (1990). DNA sequencing separations in capillary gels on a modified commercial DNA sequencing instrument. *Biotechniques* **9**:74–79.

Zander, C, Drexhage, KH, Han, KT, Wolfrum, J, and Sauer, M (1998). Single-molecule counting and identification in a microcapillary. *Chem Phys Lett* **286**:457–465.

Zander, C, Enderlein, J, and Keller, RA, eds. (2002). *Single Molecule Detection in Solution: Methods and Applications*. Wiley-VCH, Berlin.

Zhang, J, Voss, KO, Shaw, DF, Roos, KP, Lewis, DF, Yan, J, Jiang, R, Ren, H, Hou, JY, Fang, Y, Puyang, X, Ahmadzadeh, H, and Dovichi, NJ (1999). A multiple-capillary electrophoresis system for small-scale DNA sequencing and analysis. *Nucleic Acids Res* **27**:e36–e36.

Zhang, JZ, Yang, MJ, Puyang, XL, Fang, Y, Cook, LM, and Dovichi, NJ (2001). Two-dimensional direct-reading fluorescence spectrograph for DNA sequencing by capillary array electrophoresis. *Anal Chem* **73**:1234–1239.